EUROFUSION WP14ER-PR(15) 13840

A Shalpegin et al.

Highly resolved stereoscopic measurements of dust motion in the sheath boundary of magnetized plasmas

Preprint of Paper to be submitted for publication in Nuclear Fusion

This work has been carried out within the framework of the EUROfusion Consortium and has received funding from the Euratom research and training programme 2014-2018 under grant agreement No 633053. The views and opinions expressed herein do not necessarily reflect those of the European Commission.

Highly resolved stereoscopic measurements of dust motion in the sheath boundary of magnetized plasmas

A. Shalpegin[1,2], F. Brochard[1], S. Ratynskaia[3], P. Tolias[3], M. De Angeli[4], L. Vignitchouk[3], I. Bykov[3], S. Bardin[5], K. Bystrov[5], T. Morgan[5], G. De Temmerman[6]

[1] *Université de Lorraine, Institut Jean Lamour, UMR 7198 CNRS, Vandoeuvre-lés-Nancy, France*

[2] *IGVP, Universität Stuttgart, Pfaenwaldring 31, 70569, Stuttgart, Germany*

[3] *KTH Royal Institute of Technology, Association EUROfusion-VR, Stockholm, Sweden*

[4] *Istituto di Fisica del Plasma - Consiglio Nazionale delle Ricerche, Milan, Italy*

[5] *FOM Institute DIFFER - Dutch Institute for Fundamental Energy Research, Partner in the Trilateral Euregio Cluster, The Netherlands*

[6] *ITER Organization, Route de Vinon-sur-Verdon, CS 90 046, 13067 St Paul Lez Durance Cedex, France*

Dust trajectories have been recorded with an unprecedented, under fusion-relevant plasma conditions, spatial resolution of 9 μm/pixel in Pilot-PSI. The optical set-up allowed the use of fast cameras as a basic microscope. It is demonstrated that such a resolution is essential for the correct interpretation of experiments on several aspects of dust-surface interactions. Highly resolved tungsten dust dynamics measurements are presented from dedicated experiments on dust collisions with plasma facing components, motion in the vicinity of castellated samples and remobilization from planar samples.

Direct visualization of dust dynamics has been a driving force in the development of complex plasmas, camera observations of dust acoustic waves [1] and particle kinetics in the crystalline and liquid phases [2] serve as prominent examples. In complex plasma experiments, dust is injected into the small volume of a low temperature discharge and visualization is achieved with the use of laser illumination; a laser beam is transformed into a thin sheet that illuminates the grains and the scattered light is recorded [3]. Direct visualization of dust dynamics has also been a crucial tool for understanding dust transport in fusion devices [4, 5]. In fusion plasmas, owing to the large device size, laser illumination is prone to low dust detection probability [6], unless the beam cross-section is large [7]. Visualization is usually achieved by capturing thermal radiation emitted by dust grains, taking advantage of the high surface temperature that the grains can reach by absorbing plasma fluxes. The typical spatial resolution is relatively low ($\sim$ few mm/px) due to the large distances to the volume of interest and the limited access of cameras. Nevertheless, it proved sufficient for successful stereoscopic measurements (NSTX [8], MAST [9], ASDEX Upgrade [10]) that confirmed the dominant role in dynamics of the ion drag force and of centrifugal effects due to the curved flow.

On the other hand, in order to correctly interpret observations of phenomena related to dust dynamics in the vicinity of plasma-facing components (PFCs), a much higher resolution is required. **(i)** Dust-PFC mechanical impacts are unavoidable in fusion devices and have been demonstrated to be a controlling factor of dust migration around the torus [11]. They are described by restitution coefficients, *i.e.* ratios of the impact to the rebound velocities, for the normal and tangential to the impact plane components [11, 12]. As a consequence of the omnipresent ion-scattering and electrostatic forces, whose expressions near the PFC boundary are unknown and thus cannot be extracted from observations, experimental restitution curves require high spatial and temporal resolution [13]. **(ii)** Dust dynamics in the vicinity of castellated PFCs [14] have strong implications for the development of *in situ* dust removal techniques. The gap width in ITER will be 500 μm, thus a much smaller resolution is desirable. **(iii)** The remobilization of dust grains adhered to PFCs plays an important role in a wide range of issues ranging from dust accumulation site formation to in-plasma dust lifetime estimation. Recently, different remobilization conditions have been formulated that refer to detachment, sliding or rolling [15]. However, it has not been possible to determine which of these conditions is first realized in remobilization activity observed in experiments. **(iv)** Metallic dust / droplet formation mechanisms under transient ITER-relevant conditions need to be identified and quantified. Enhanced resolution is a necessary ingredient of experimental studies of dust production from PFC cracking [16, 17] and droplet release from melt-layer splashing [18–20], since it can allow for the estimation of the amount and ejection velocity of grains, but also of the moment of formation and ejection.

Despite their diversity, all aforementioned phenomena involve the dust-PFC contact, which implies that the desired resolution is close to the grain size. Such a resolution is unattainable in tokamaks, but it can be achieved in linear plasma simulators which combine optimized diagnostic access, well-confined plasma columns and lower - compared to tokamaks - external magnetic fields, characteristics that are essential for a highly resolved stereoscopic reconstruction of dust trajectories. In this Letter, we demonstrate how to achieve a resolution of a few micrometers per pixel even in relatively large devices. We present finely resolved dust measurements in boundary-sheath plasmas. In particular, we focus on dust-PFC impacts, motion in the vicinity of castellated bound-

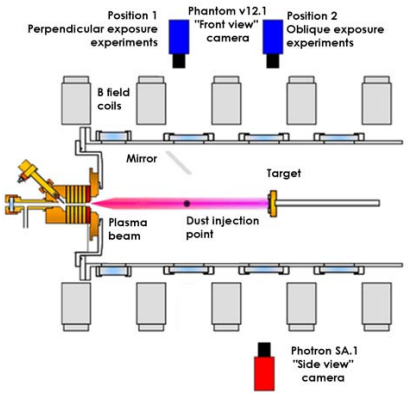

FIG. 1: Schematic of Pilot-PSI with the camera arrangement.

aries and remobilization from planar boundaries. The experiments were carried out in Pilot-PSI [21, 22], a device uniquely capable of reproducing the ITER divertor plasma conditions.

Plasma (hydrogen here) is generated by a cascaded arc source that exhausts into a 40 cm diameter vacuum vessel and is confined by a strong axial magnetic field, resulting in a Gaussian-profile beam with a full width at a half maximum $\sim$ 1 cm. The plasma parameters have a weak axial dependence and also depend on the applied magnetic field which in our experiments varied in the range of $B = 0.4 - 1.2$ T. At the center of the column, the plasma density is $\sim 10^{20} - 10^{21}\,\mathrm{m}^{-3}$ and the electron temperature ~ 2 eV. Spherical nearly monodisperse tungsten (W) dust of 9 μm diameter was injected by means of a dust dropper installed in the middle top beam port [13]. A mirror polished W target was exposed perpendicularly to the B-field in experiments dedicated to dust-PFC collisions, whereas two $23 \times 23 \times 10\,\mathrm{mm}^3$ flat W monoblocks separated by a 0.5 mm gap were exposed perpendicularly in experiments dedicated to the study of dust motion near castellated PFCs. Simulations with the MIGRAINe dust dynamics code have revealed that the injected dust grains reach the targets after multiple impacts with the vessel, passing through the plasma column several times [13]. Despite being of the same size, they follow different paths which results in different velocities and bulk temperatures when impinging on the target. Finally, planar W samples with pre-adhered dust grains were employed for remobilization experiments and exposed in dust-free discharges both normal and oblique (10°) with respect to the B-field, see Fig.(1). Two high-speed visible range cameras were used for the observation of a small volume in front of the target: Photron FASTCAM SA1.1 ("side view" camera) and Phantom v12.1 ("front view" camera), as shown in Fig.(1).

The "side-view" camera provided a view parallel to the target's surface, both in the vertical and oblique configurations, directly through the window near the target. The camera was equipped with one Nikon 200 mm f/4 ED-IF AF Micro-NIKKOR telephoto lens and an additional set of teleconverter lenses (2x Nikon AF-S Teleconverter TC-20E III and Kenko 2x NAS MACRO TELEPLUS MC7). The camera and optics were mounted on an optical rail, which proved to be a stable and flexible solution concerning position adjustments. A particular advantage of the main lens is that it's minimal focusing distance is 0.5 m which alone leads to the high resolution of 20 μm/px at this distance. The magnification of an optical system in a zero order approach is given by $M = f/(f - d)$, where M, f, d are the magnification, focal length and distance to the observed object, respectively. The teleconverter lenses increased the effective focal length by a factor of four without changing the minimal focusing distance, thus, significantly enhancing the spatial resolution. No noticeable aberrations have been introduced by the additional teleconverter lenses, although they led to a decrease of the image brightness equivalent to two stops of the aperture for each added lens. The optimal distance between the camera and the target was defined by two major limitations: (i) the geometry of vacuum vessel and the viewing ports, (ii) the maximum value of the stray magnetic field tolerated by the camera. See Table I for the highest resolution achieved by the side-view set-up.

TABLE I: The optimal spatial resolution achieved by the "side view" optical system for different magnetic fields.

B (T)	d (m)	stray-B (mT)	resolution (μm/px)
0.4	0.65	2.11	9
0.8	0.8	2.08	13
1.2	1.2	2.20	20

The "front-view" camera was observing the target's surface exposed to plasma in Position 1 and 2 of Fig.(1). The camera was equipped with a AF DC-Nikkor 135 mm $f/2D$ lens and a set of H_α, H_β notch filters to decrease the pollution of the observed volume by plasma light. The relatively low focal length of the lens and the enlarged, due to the mirrors, camera-target distance limited the optimal spatial resolution to 100 μm/px. Therefore, the data obtained by this camera are mainly used only as a reference for general characteristics of the dust motion.

The recorded videos were analysed with the TRACE code [23], which processes high speed videos on a frame-by-frame basis, detects pinpoint bright events, classifies and arranges them into trajectories. All videos were pre-processed in order to increase the efficiency of the dust tracking algorithm. The background was removed to increase the contrast of the frames. Dash-like tracks of fast moving grains were replaced by their geometrical centre of mass. In some cases, a single frame contained the image of a moving grain before and after the impact with the target, resulting in a V-shaped track. In such cases, the velocity prior and post impact was calculated based on the track lengths. We note that the size of the dust image on a frame is defined by a combination of the dust velocity, the camera spatial resolution and the sensor ex-

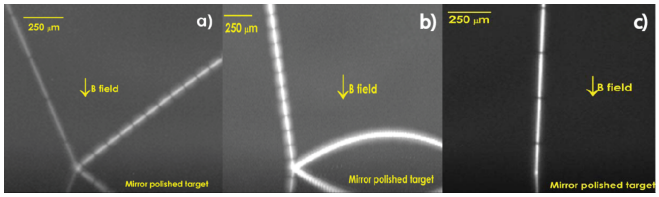

FIG. 2: Dust-surface collisions. Typical trajectories in case of (a) small loss of normal velocity, (b) substantial loss of normal velocity, (c) sticking.

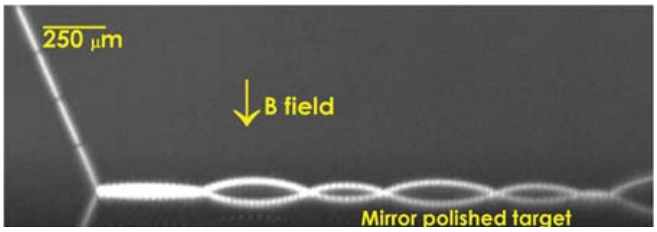

FIG. 3: An impact accompanied by multi-bouncing.

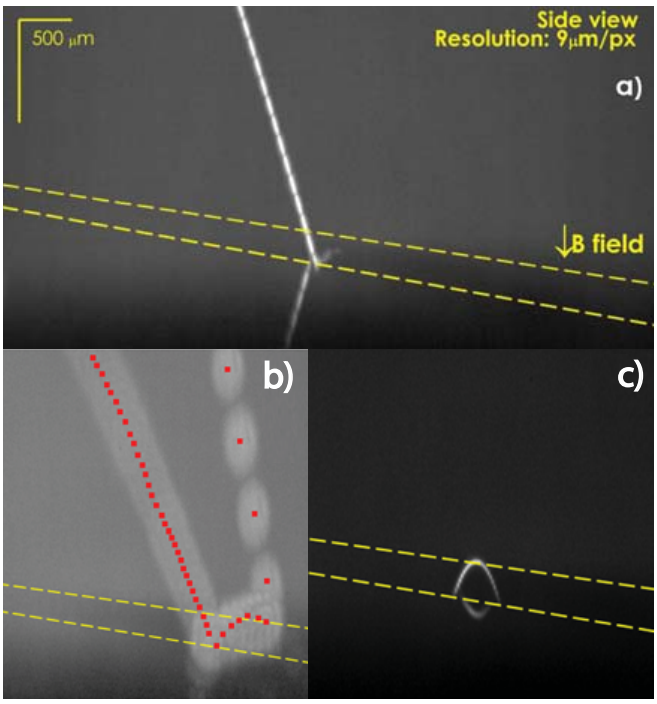

FIG. 4: Dust motion near castellated targets, the yellow dashed lines indicate the gap edges. (a) Dust moves directly into the gap, two reflection tracks are visible; from the top and the side of the gap. (b) Dust collides with the far gap edge, crosses the gap, collides with the second gap edge and escapes. The grain's image is blurred due to the fact that it is out of focus, the positions are marked by red dots. (c) Dust residing in the gap remobilizes, comes out of the gap and is pushed back by the plasma.

posure time. Here we shall present typical observations made with a spatial resolution of 9 μm/px and a temporal resolution of 33 μs, the field of view of the side camera is 720×192 pixels. Notice that, for mirror-polished targets, the reflections of the dust grain are also visible.

For the study of in-plasma dust-surface collisions more than 400 impacts have been analyzed that can be classified into three major groups. The impact velocities lie in the range $0.1 - 25$ m/sec. *(i) Rebound with small dissipation of the normal impact velocity component.* In the majority of impacts $\gtrsim 60\%$, the tangential component of the dust velocity is nearly conserved, whereas the normal velocity is decreased by a small portion, see Fig.(2a). Such a trend qualitatively agrees with the dust-surface interaction model incorporated in the MIGRAINe code [11, 12], according to which the dissipation of the normal impact velocity due to adhesive and plastic work [24] is much bigger than the negligible dissipation of the tangential impact velocity due to friction. *(ii) Rebound with large dissipation of the normal impact velocity component.* In $\sim 20\%$ of impacts, a significant part of the normal velocity is lost, whereas the tangential velocity is still conserved, see Fig.(2b). Enhanced kinetic energy losses due to plastic work indeed occur at higher dust bulk temperatures [12], as a consequence of the large decrease of the yield strength of tungsten [25]. Few of the events of this group are characterized by multi-bouncing; the normal rebound velocities are so low that momentum exchange with the ions can drag the dust back to the surface. Such an instance is depicted in Fig.(3). *(iii) Sticking.* In the remaining $\sim 20\%$ of impacts, the dust grains stick to the surface and rapidly cool, see Fig.(2c). Upon contact, the brightness of the dust images drops to the background emission level within several tens of μs, which corresponds to $1 - 2$ integration times of the camera's sensor. In almost 90% of these events, the impact speed is relatively high ($10 - 20$ m/s) and the dust trajectories are nearly normal to the target sampling denser and hotter plasma. Hence, these grains are characterized by elevated bulk temperatures and enhanced plastic deformation which prevents their rebound. Finally, in $\sim 1\%$ of impacts, one of the velocity components significantly increases. Two mechanisms can be responsible for these rare events: either dust encountered some sparse irregularities on the mirror-polished surface or dust was spinning prior to the collision instant and the impact dynamics allowed for a transfer of kinetic energy from the rotational to the translational degrees of freedom.

Examples of dust motion in the vicinity of castellations are presented in Fig.(4). Despite the fact that the gap width is hundreds of times larger than the Debye length, the presence of the gap does not influence dust trajectories. Moreover, only a small dust fraction ends up inside the gap, consistent with geometrical arguments considering only the relative area. However, these conclusions should not be perceived as generic, since in the particular set-up, most of the grains arrive at the castellated surface with predominantly normal speeds. For dust grains arriving with strong tangential components, rebounding in the vicinity of castellations might provide an effective

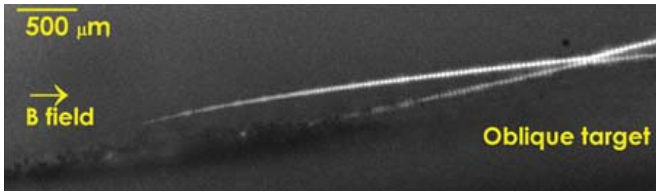

FIG. 5: Dust remobilization in the oblique configuration.

mechanism of gap trapping.

Dust remobilization by plasma forces can be experimentally studied in a systematic manner by a recently developed technique based on controlled adhesion via gas-dynamic methods [15]. The trajectory of a dust grain that remobilized from a mirror polished W surface with pre-adhered W dust spots is shown at Fig.(5). The initial part of the trajectory is not visible, since the grain was not incandescent enough. Therefore, it is not possible to infer which of the remobilization conditions is realized. Notice that the remobilized grain subsequently collides with the target and bounces off.

It is worth briefly returning to Fig.(3) in order to demonstrate how insufficient resolution can lead to misinterpretations. In the normal direction, the observed multi-bouncing can be viewed as an oscillation with an amplitude less than $50\,\mu$m. Consequently, with a resolution $> 100\,\mu$m/px, one would deduce that the grain is sliding / rolling along the surface of the target, somehow remaining hot, despite having established a mechanical contact with the actively cooled target. In our previous experiments with $\sim 200\,\mu$m/px resolution, we had indeed encountered such "seemingly paradoxical" trajectories [13].

To sum up, an unprecedented spatial resolution of $9\,\mu$m/px has been achieved under fusion relevant conditions. Such a high resolution is essential for the correct interpretation of experiments focusing on aspects of in-plasma dust-surface interactions. This is demonstrated by experiments on mechanical dust-surface collisions, dust motion in the vicinity of castellations and dust remobilization. Application of the technique presented here will not only allow for the calibration of analytical dust-surface impact models but also assist in shedding light on a number of unresolved ITER-relevant issues, such as the clarification of the mechanisms leading to dust amassment in the grooves of castellated PFCs, the determination of dust remobilization conditions and the quantification of dust production mechanisms.

Acknowledgments. A.S would like to acknowledge the support of the Erasmus Mundus International Doctoral College in Fusion Science and Engineering (FUSION-DC). This project has received funding (Enabling Research project CfP-WP14-ER-01/VR-01) from the European Unions Horizon 2020 research and innovation programme under grant agreement number 633053. The views and opinions expressed herein do not necessarily reflect those of the European Commission.

[1] A. Barkan, R. L. Merlino and N. D'Angelo, Phys. Plasmas **2**, 3563 (1995).
[2] G. E. Morfill and A. V. Ivlev, Rev. Mod. Phys. **81**, 1353 (2009).
[3] V. E. Fortov, A. V. Ivlev, S. A. Khrapak, A. G. Khrapak, and G. E. Morfill, Phys. Rep. **421**, 1 (2005).
[4] S. I. Krasheninnikov, R. D. Smirnov and D. L. Rudakov, Plasma Phys. Control. Fusion **53**, 083001 (2011).
[5] S. Ratynskaia, C. Castaldo, H. Bergsåker, D. Rudakov, Plasma Phys. Control. Fusion **53**, 074009 (2011).
[6] D. L. Rudakov, J. H. Yu, J. A. Boedo *et al.* Rev. Sci. Instrum. **79**, 10F303 (2008).
[7] M. Kantor, M. Tsalas, A. Litnovsky *et al.*, J. Nucl. Mater. **438**, S711 (2013).
[8] J. Nichols, A. L. Roquemore, W. Davis *et al.*, J. Nucl. Mater. **415**, S1098 (2011).
[9] G. De Temmerman, M. Bacharis, J. Dowling and S. Lisgo, Nucl. Fusion **50**, 105012 (2010).
[10] Z. Yang, K. Krieger, T. Lunt *et al.*, J. Nucl. Mater. **438**, S846 (2013).
[11] S. Ratynskaia, L. Vignitchouk, P. Tolias *et al.*, Nucl. Fusion **53**, 123002 (2013).
[12] L. Vignitchouk, P. Tolias and S. Ratynskaia, Plasma Phys. Control. Fusion **56**, 095005 (2014).
[13] S. Ratynskaia, P. Tolias, A. Shalpegin *et al.* J. Nucl. Mater. dx.doi.org/10.1016/j.jnucmat.2014.09.064.
[14] R. A. Pitts, S. Carpentier, F. Escourbiac *et al.*, J. Nucl. Mater. **438**, S48 (2013).
[15] P. Tolias, S. Ratynskaia, M. De Angeli *et al.*, Nucl. Fusion (submitted).
[16] V. A. Makhlaj, I. E. Garkusha, N. N. Aksenov *et al.*, J. Nucl. Mater. **438** S233 (2013).
[17] A. Suslova, O. El-Atwani, S. S. Harilal and A. Hassanein, Nucl. Fusion **55**, 033007 (2015).
[18] N. Klimov, V. Podkovyrov, A. Zhitlukhin *et al.*, J. Nucl. Mater. **390-391**, 721 (2009).
[19] K. Krieger, T. Lunt, R. Dux *et al.*, Phys. Scr. **T145**, 014067 (2011).
[20] G. De Temmerman, J. Daniels, K. Bystrov, M.A. van den Berg and J.J. Zielinski, Nucl. Fusion **53**, 023008 (2013).
[21] G. J. van Rooij, V. P. Veremiyenko, W. J. Goedheer *et al.*, Appl. Phys. Lett. **90**, 121501 (2007).
[22] G. De Temmerman, J. J. Zielinski, S. van Diepen *et al.*, Nucl. Fusion **51**, 073008 (2011).
[23] S. Bardin, J.-L. Briancon, F. Brochard *et al.*, Contrib. Plasma Phys. **51**, 246 (2011).
[24] C. Thornton and Z. Ning, Powder Technol. **99**, 154 (1998).
[25] A. Luo, K. S. Shin and D. L. Jacobson, Scr. Metall. Mater. **25**, 2411 (1991).